RL-82-051

Science and Engineering Research Council
Rutherford Appleton Laboratory
CHILTON, DIDCOT, OXON, OX11 0QX

RL-82-051

Measurements of Water Vapour Absorption in the RAL Untuned Cavity

R.J.Knight, D.T.Llewellyn-Jones

July 1982

RESEARCH NOTE

REPORT ON MEASUREMENTS OF WATER VAPOUR ABSORPTION IN THE RAL UNTUNED CAVITY, 1981

R J Knight
D T Llewellyn-Jones

Rutherford Appleton Laboratory
Chilton
DIDCOT
Oxon
OX11 0QX
UK

Introduction

A large untuned resonant cavity has been used to measure the absorption coefficient of air-broadened water vapour as a function of frequency, water vapour partial pressure and temperature. The measured absorption is greater than is predicted from the AFGL (Ref. 22) line data and the Gross (Ref. 23) line shape*, the excess having a quadratic dependence on water content and a negative temperature coefficient. It has been found that this temperature coefficient is not constant with frequency. Comparisons are made with field measurements, and empirical formulae given for propagation predictions.

Millimetre-wave propagation through the clear atmosphere is strongly influenced by oxygen and water vapour. Oxygen has an absorption line at 118.75 GHz and a number of lines clustered around 60 GHz, which at atmospheric pressure are broadened into a single feature. Water vapour has absorption lines centered at 22.235 GHz and 183.31 GHz, with a large number of lines at higher frequencies whose wings contribute to the microwave and millimetre absorption. There are also some weak lines at low frequencies. Other atmospheric constituents have a negligible effect in this region at ground level. It is a common observation (Ref. 1-3) that measured absorption levels in the window regions between these lines, both in the microwave and infrared, are higher than predictions, and there are a number of hypotheses to account for this. One assumption is an incorrect line shape (Ref. 4), others that the excess absorption is due to aggregates of water vapour; either dimers, polymers or clusters (Ref. 5-7). More than one of these may be present, and different causes may apply in different frequency regions. In order to understand the mechanisms involved, it is necessary to have precise absorption measurements as a function of frequency, temperature and water content.

* A standard procedure for computing molecular absorption

The Untuned Cavity

In the microwave and millimetre region attenuation levels in the absorption windows are low, of the order 0.1 to 1.0 dB/km, thus long path lengths are necessary. In the atmosphere, homogenity cannot be guaranteed, and there is no control over the meteorological parameters. Other effects such as scattering, stray reflections, scintillation and precipitation may distort measurements. In the laboratory, obtaining a long path conveniently is difficult at low frequencies. Multiple pass cells, such as the White (Ref. 8) cell (which can be regarded as a folded Fresnel lens system) used in the visible and infrared are limited by diffraction in the number of images obtainable. (To get a 500 m path length at 100 GHz would require mirrors 300 cm diameter, in a 8 m long White cell).

Resonant cavities and Fabry Perot interferometers (Ref 9, 10) have a very narrow bandwidth, and require elaborate and precise microwave techniques, as well as retuning for varying sample quantities. The untuned resonator, however, can overcome all these difficulties. This technique was adapted from acoustic applications and used by Becker and Autler (Ref. 11), in the first laboratory measurements of absorption by the 22 GHz water vapour line. There were prompted by the mysterious failure of K-band radar to perform effectively in temperate climate. The measurements were reported in 1946 and are still regarded as definitive.

The resonator consists of a reverberant enclosure with highly reflecting walls; a mechanical stirrer performs a mode mixing function. Energy is directed into the cavity by means of a small horn, while a detector samples the level of electromagnetic radiation within the cavity (Fig. 1). The detected energy is proportional to the cavity Q, and any loss introduced into the cavity lowers the Q and hence the received signal. Calibration is achieved by opening an aperture in the wall, the theoretical loss being predicted from the aperture dimensions. The cavity behaves as an absorption cell whose pathlength corresponds to the distance travelled by a photon in the characteristic reverberation time, with no limitations set by diffraction. The high density of resonant modes, and the mixing effect of the mechnical stirrer, gives a Q which varies smoothly with frequency. There is some residual structure in the frequency dependence of the Q which can be removed by sweeping the measurement frequency by a small amount (Fig. 4). At this laboratory we have used cavities at frequencies between 10 GHz and 1000 GHz. A further advantage of the wide bandwidth is that the source stability need be no better than that of the phenomenon being studied, and elaborate frequency stabilisation techniques are not essential.

Equipment

The large untuned resonator at RAL consists of a copper cylinder with domed ends, 2 m diameter and 4 m long. The inside is silver plated to improve the reflectivity. The Q value is about 8×10^5 at 70 GHz, giving an effective path length of about 500 m. The mode stirrer consists of a four bladed paddle, with the angles of the blades adjustable to increase the uniformity of the energy distribution within the cavity. The blades fold down so the stirrer can be inserted and removed through the 30 cm diameter end hole (Fig. 2).

Temperature control is provided by a refrigeration and heating system pumping a 50% antifreeze/water mixture around external copper coils. A separate air temperature controller and humidifier/dryer circulates the air through the cavity in a closed system. Thermal insulation is provided by two 5 cm thick layers of foil backed fibre insulation which enables the temperature to be maintained constant to within 0.1 deg over the range 310K to 265K. Further thermal insulation will allow the lower limit to be extended to 240K. The humidity can be maintained to ±2% RH over the range ∿ 10% to ∿ 90%. Temperatures are monitored by an array of thermocouples mounted on the tanks external surface while the humidity is measured by an aspirated psychrometer. The calibration factor for this was obtained by transmission measurements through the cavity on the 1.4 μ water vapour absorption band (Ref. 20).

The detector used is a golay cell, which is a widely used infrared detector with room temperature operation, and whose sensitivity extends well into the microwave region. Most of the time two detectors at different locations were used, and the outputs summed, although individual measurements with the two detectors were in agreement to 0.2%. The detector outputs are fed to lock-in amplifiers and then to a chart recorder (Fig. 3).

Since the voltage output of the detector is proportional to the input power, the measured loss can be converted to attenuation by the formula, derived from equations given by Lamb (Ref. 21) :

$$\alpha\ (\mathrm{cm}^{-1}) = \frac{1}{\text{path length}} \left[\frac{\text{Initial signal}}{\text{Signal with lossy gas}} - 1\right] \qquad (1)$$

where the path length corresponding to the initial conditions is given by :

$$\text{path length} = \frac{4 \times \text{cavity volume}}{\text{Hole area}} \left[\frac{\text{Initial signal}}{\text{Signal with hole open}} - 1\right] \qquad (2)$$

Theoretical Prediction

There is much confusion about the exact form of absorption line profiles: we define the absorption coefficient of gas molecules as a function of frequency by :

$$\alpha(\nu) = A\,\nu\, f(\nu, \nu_o) \qquad (3)$$

ν_o is the line centre frequency. A is related to the number density of absorbers n, and the integrated line strength S by (Ref. 17) :

$$nS = A\,\Delta\nu\,\nu_o \qquad (4)$$

where $\Delta\nu$ is the line width.

Absorption due to molecular oxygen was calculated using the Rosenkranz formulation (Ref. 18) with the values of the interference coefficients and temperature dependences from Liebe (Ref. 19) Here :

$$f(\nu, \nu_o) = \frac{1}{\pi}\,\frac{\nu}{\nu_o}\left[\frac{\Delta\nu - (\nu_o - \nu)\,I_o}{(\nu_o - \nu)^2 + \Delta\nu^2} + \frac{\Delta\nu - (\nu_o + \nu)\,I_o}{(\nu_o + \nu)^2 + \Delta\nu^2}\right] \qquad (5)$$

where I_o is the interference coefficient, which represents the effect on an absorption line of all the other overlapping oxygen lines.

For water vapour the Gross (Ref. 23) line shape was used

$$f(\nu, \nu_o) = \frac{4}{\pi}\left[\frac{\nu\,\nu_o\,\Delta\nu}{(\nu_o^2 - \nu^2)^2 + 4\Delta\nu^2\,\nu^2}\right] \qquad (6)$$

with over 500 lines from the AFGL 1980 line data tape (Ref. 22)

The effective broadening of the water vapour includes the self broadening (about 5 times that of the foreign gas broadening).

Experimental Results

At each frequency, calibration was performed by measuring the loss of energy through an aperture of known area. This is converted into an effective path length (Eqn. 2) at the temperature, humidity and total pressure at the time of the measurement.

At each frequency measurements of water vapour loss were made at different temperatures, several runs at each temperature. The time taken for the temperature to stabilize was up to 6 hours, and the cavity was being dried during this time. Zero humidity cannot be reached, thus the starting conditions, always less than 10% RH, were different from run to run depending upon the length of drying. As humidification took place, the signal was seen to drop, and at each measurement point humidification was stopped until stable conditions were reached, usually only a few minutes. The psychrometer readings were taken, together with the averaged cavity temperature reading from the thermocouples. Humidification was stopped around 80% RH and then the cavity was dried in stages, with further measurements being taken. The analysis was taken from the chart record of detector signal using (Eqn. 1). By a series of comparisons of the effect of changing the humidity of the air inside the cavity with that of opening a calibrating aperture of known area, and extrapolation to zero humidity, it is possible to obtain data in the form shown in Figs. 5 and 6 where the component of absorption due to water vapour is shown as a function of the absolute humidity of the air, and as a function of temperature. The oxygen attenuation is virtually constant for the duration of each run; a slight correction is necessary because of the difference between water vapour/oxygen and nitrogen/oxygen broadening. This is of the order of 7×10^{-4} km^{-1} $mbar^{-1}$ at 67 GHz and less at other frequencies. The predicted water vapour attenuation was subtracted from all measured values, and curves fitted to the excess. All the curves showed pronounced quadratic pressure dependence of excess absorption upon water vapour concentration. Calculation of the loss is accurate to about 7% for each point, thus it is not possible to decide if there is a linear contribution as well.

The measurement temperature was taken to be the closest 0.5° to the average temperature over one run. It is found that the temperature dependence of the excess absorption can be described by an empirical term of the form

$$\rho \text{ excess} = A\rho^2 \exp\left[B\left(\frac{1}{T} - \frac{1}{300}\right)\right] \qquad (7)$$

where ρ is the water amount in gm/m^3.

By using Eqn. (7) the individual data points are temperature corrected to the value taken for the measurement temperature, and the whole process iterated until there is convergence. The overall change in the values of the constants A and B in Eqn. (7) is about 10% from beginning to end, the final values of A and B being given in Table 2.

Table 2

Frequency (GHz)	A [dB km^{-1} $(gm.m^{-3})^{-2}$]	B [deg/molecule]
29.9	8.57×10^{-4}	7242
67.7	1.57×10^{-3}	7950
69.3	1.62×10^{-3}	7555
110.0	3.60×10^{-3}	4039

The frequency dependence of the excess absorption may be empirically fitted by the equations :

$$A = 1.36 \times 10^{-5} \nu + 1.68 \times 10^{-7} \nu^2 \qquad (8)$$

$$B = 8008 - 1.282 (\nu - 54.3)^2 \qquad (9)$$

where ν is frequency in GHz.

These curves are plotted in Fig. 8, together with the measured points. It is obviously unwise to extrapolate too much beyond the limits of frequency covered by these measurements.

Comparison with other Measurements

This first set of data enables a more accurate prediction of microwave molecular absorption due to water vapour than has previously been possible.

It is difficult, however, to find data in the literature with which to compare it. Most published measurements are in obscure reports, and compilations with poor quality graphs have been composed of widely differing data, converted to a standard temperature and water amount by arbitrary means. The first comparison here is with laboratory data: the measurements of Becker and Autler in 1946 (Ref. 11). These were the first untuned resonator measurements, and were at 45°C from 18 - 40 GHz. The excess absorption from their data is plotted in Fig. 9, with the curve derived from equations 7 - 9. The second comparison is with free space measurements at 70 - 80 GHz by Hogg (Ref. 13). These comprise a set of a years data, to encompass the range of humidity. Unfortunately, there is no temperature information. Fig. 10 has their data points, together with curves from equations (7 - 9) for a number of temperatures, the assumption being that there is a general increase in temperature with increasing humidity. The fit is reasonably good at 70 GHz but overestimates the attenuation at 79 GHz, showing the dangers of interpolating excess absorption measurements.

There are more measurements available of zenith attenuation; however we need information on the variation of excess absorption with total pressure. If excess absorption were due solely to the wings of far lines then it would be proportional to the total pressure, and the excess at zero broadening would be small. If, on the other hand, it were due to an additional species such as dimers or clusters it would not necessarily be expected to show strong dependence on total pressure. The few laboratory measurements that have been done in this region (unpublished RAL measurements) show that the ratio of excess absorption with no foreign gas broadening to that with 1 atmosphere of air is variable with frequency, and is not necessarily a smooth function of pressure.

The most reliable RAL measurement is at 110 GHz, and gives an attenuation level in water vapour alone which is comparable to that reported here with 1 atmosphere broadening. If we assume that the excess absorption at this frequency is independent of total pressure, then using a representative global selection of 60 radiosonde profiles, together with Eqn. 7, we can calculate expected clear sky zenith attenuation as a function of precipitable water [Fig. 11]. Multilayer models are used; up to 14 km for water vapour and 45 km for oxygen. The scatter in the calculated values of attenuation is due to the variability in the temperature and humidity profiles; there is also some scatter in the total oxygen attenuation (0.34 - 0.43 dB). It is interesting to note that although half the absorption is given by the excess component, with a quadratic dependence upon water content, the predicted absorption appears to indicate a linear dependence. This is because increasing water amount is generally accompanied by higher temperature, and so humidity and temperature are not fully independent. This indicates that the apparent linear dependence of absorption on water content that has been reported by many authors (e.g. Ref. 13, Ref. 15) and incorporated in various empirical models (Ref. 25) is not a true representation of the actual behaviour, and can lead to erroneus predictions in some conditions of temperature and humidity. Also shown are various zenith measurements. The Texas measurements are all below the predicted curve; the single point at the end shows the effect of increasing the ground temperature from 300K to 309K.

Conclusion

The first year of operating the RAL untuned cavity has demonstrated that the facility is producing data which can be used by communications engineers for predicting the clear transmission characteristics of the atmosphere, both in terrestrial and earth-satellite propagation paths. The latter, however, will need information on atmospheric pressure dependence in order to make the most accurate predictions.

R J KNIGHT
D T LLEWELLYN JONES

February 1982

References

1. Anomalies in the Absorption of Radio Waves by Atmospheric Gases
A W STRAITON AND C W TOLBERT
PROC IRE 48 898 1960

2. Observations of Anomalous Submillimeter Atmospheric Spectra
G G GIMMESTAD et al
ASTROPHYSICAL JOURNAL 218 311 1977

3. Infrared Continuum Absorption by Atmospheric Water Vapour in the 8 - 12 μm Window
R E ROBERTS et al
APPLIED OPTICS 15 2085 1976

4. The Water Vapour Continuum as Wings of Strong Absorption Lines
R J NORDSTROM AND M E THOMAS
"Atmospheric Water Vapour" Ed A Deepak Academic Press 1980

5. Absorption of Microwaves in Air by Water Vapour Dimers
A A VIKTOROVA AND S A ZHEVAKIN
Soviet Physics Doklady 11 1065 1967

6. Resonant Absorption by Water Polymers in the Atmosphere
H A GEBBIE
Nature (to be published)

7. Ion Content and Infrared Absorption of Moist Atmospheres
H R CARLON
J Atmos Sci 36 832 1979

8. Long Optical Paths of Large Aperture
J V WHITE
J Opt Soc Am 32 285 1942

9. Microwave Spectroscopy
C H TOWNES AND A L SCHAWLOW
McGraw Hill 1955

10. A High Q Fabry Perot Interferometer for Water Vapour Absorption Measurements in the 100 GC/s to 300 GC/s range
E P VALKENBURG AND V E DERR
Proc IEEE 54 493 1966

11. Water Vapour Absorption of Electromagnetic Radiation in the Centimetre Wavelength Range
G E BECKER AND S H AUTLER
Phys Rev 70 300 1946

12. Propagation Through the Atmosphere at Frequencies greater than 10 GHz
D C HOGG
Progress in Radio Science Vol 2 49 1971 (URSI)

13. Atmospheric Emission Measurements at 85 to 118 GHz
C J GIBBINS et al
Planet Space Sci 23 61 1975

14. Solar Emission and Atmospheric Attenuation between the frequencies of 100 and 114 KMCS
C W TOLBERT et al
EERL Report 6.39 1960 (University of Texas)

15. Absolute Measurements of the Atmospheric Transparency at Short Millimetre Wavelengths
D P RICE AND P ADE
Infrared Physics 19 575 1979

16. PhD Thesis
R W SAUNDERS London 1979

17. Line Shape Functions for the Computation of the Absorption Coefficient of Water Vapour at Submillimeter Wavelengths
A J KEMP
Infrared Physics 19 595 1979

18. Shape of the 5 mm Oxygen Band in the Atmosphere
P W ROSENKRANZ
IEEE Trans AP 23 498 1975

19. Modelling Attenuation and Phase of Radio Waves in Air at Frequencies below 1000 GHz
H J LIEBE
Radio Science 16 1183 1981

20. Atmospheric Absorption by the 7250 cm^{-1} Water Vapour Band
P H MOFFAT AND W B JOHNSON
(To be published)

21. Theory of a Microwave Spectroscope
W E LAMB
Phys Rev 70 308 1946

22. AFGL Atmospheric Absorption Line Parameters Compilation 1980 version
L S ROTHMAN
App Optics 20 791 1981

23. Shape of Collision-Broadened Spectral Lines
E P GROSS
Phys Rev 97 395 1955

24. D Wark (NOAA) Private Communication

25. J W WATERS in
Methods of Expt Physics (ed M L Meeks)
Vol 12B Academic Press NY 1976

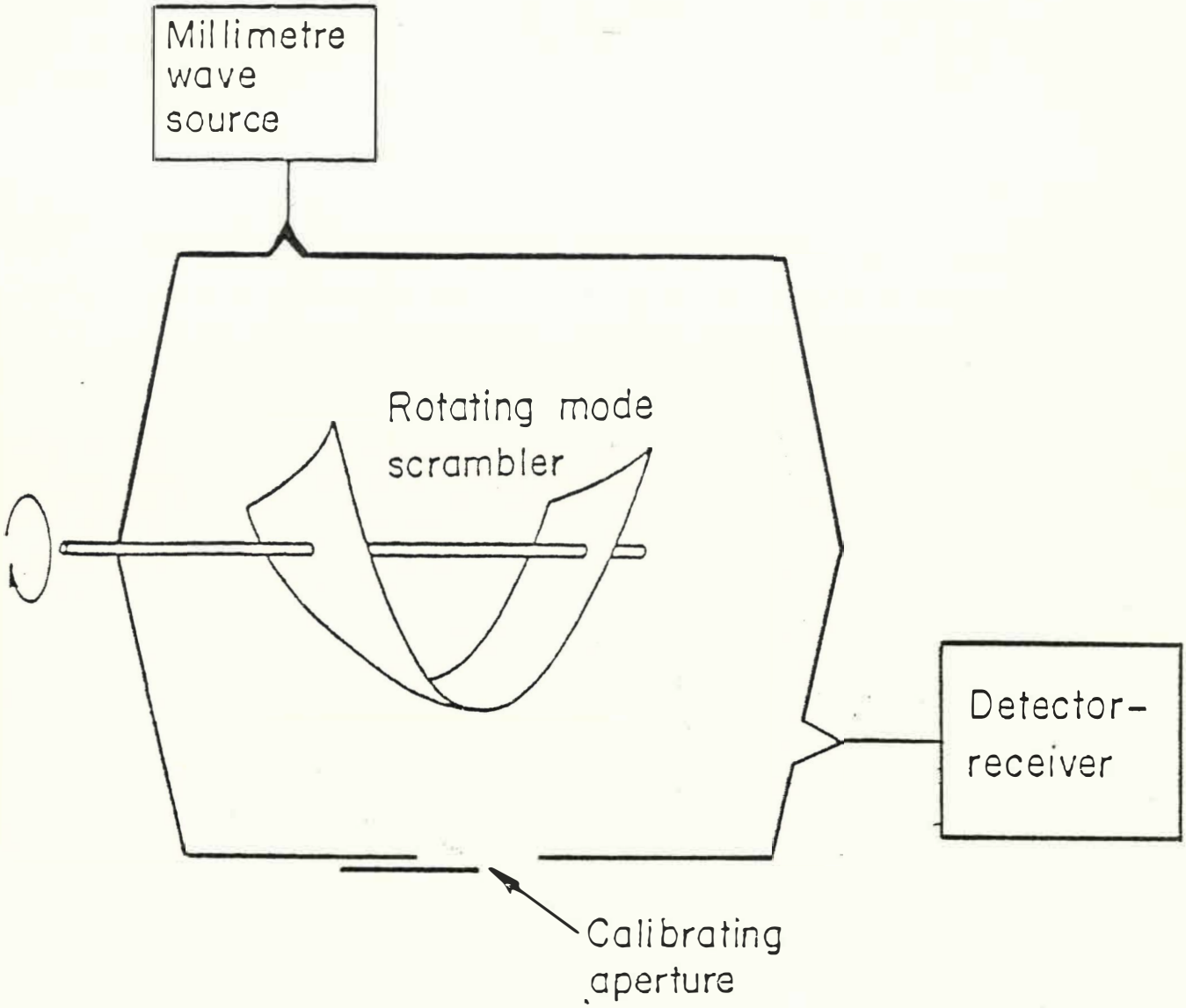

Fig. 1 Untuned Cavity

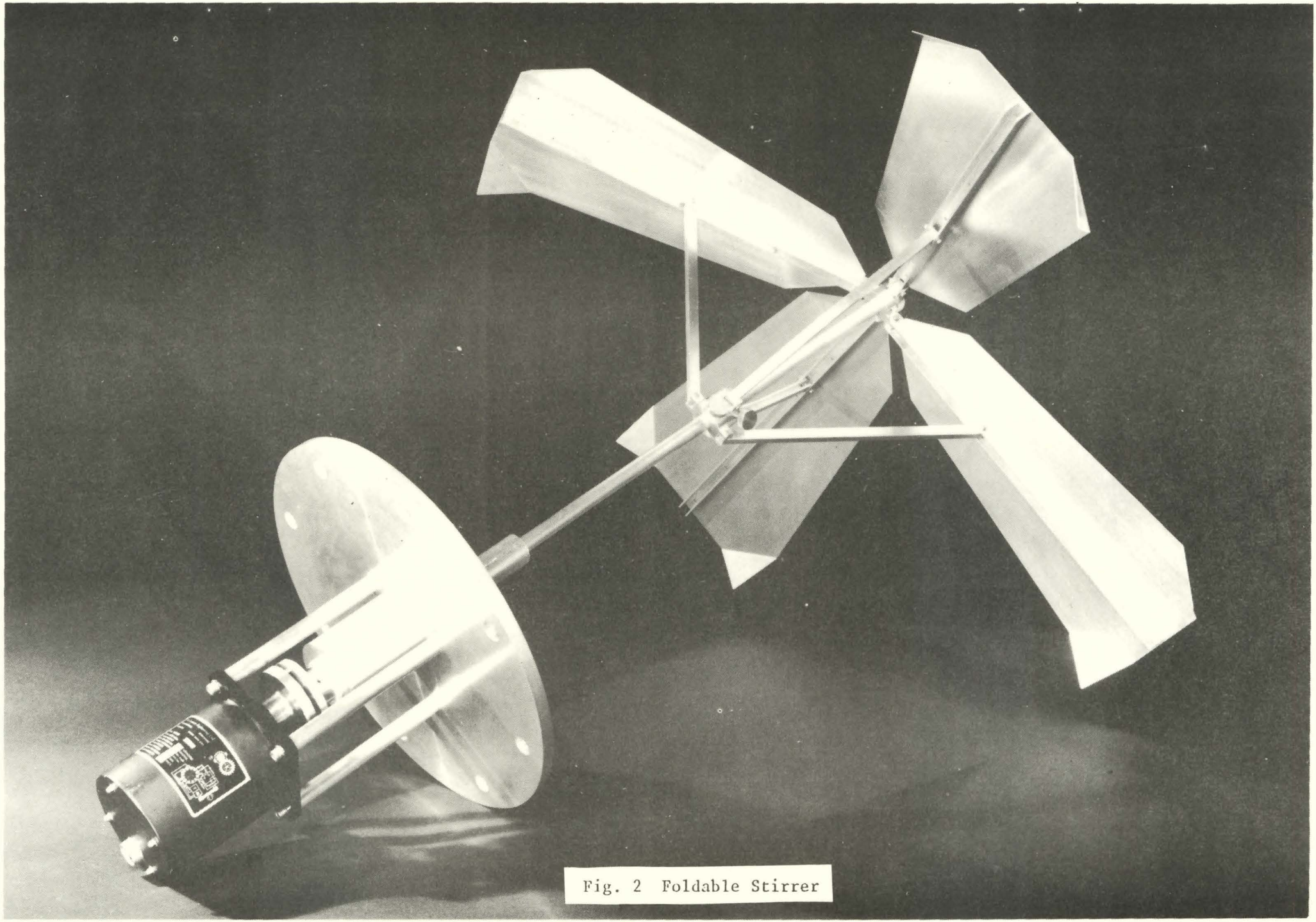

Fig. 2 Foldable Stirrer

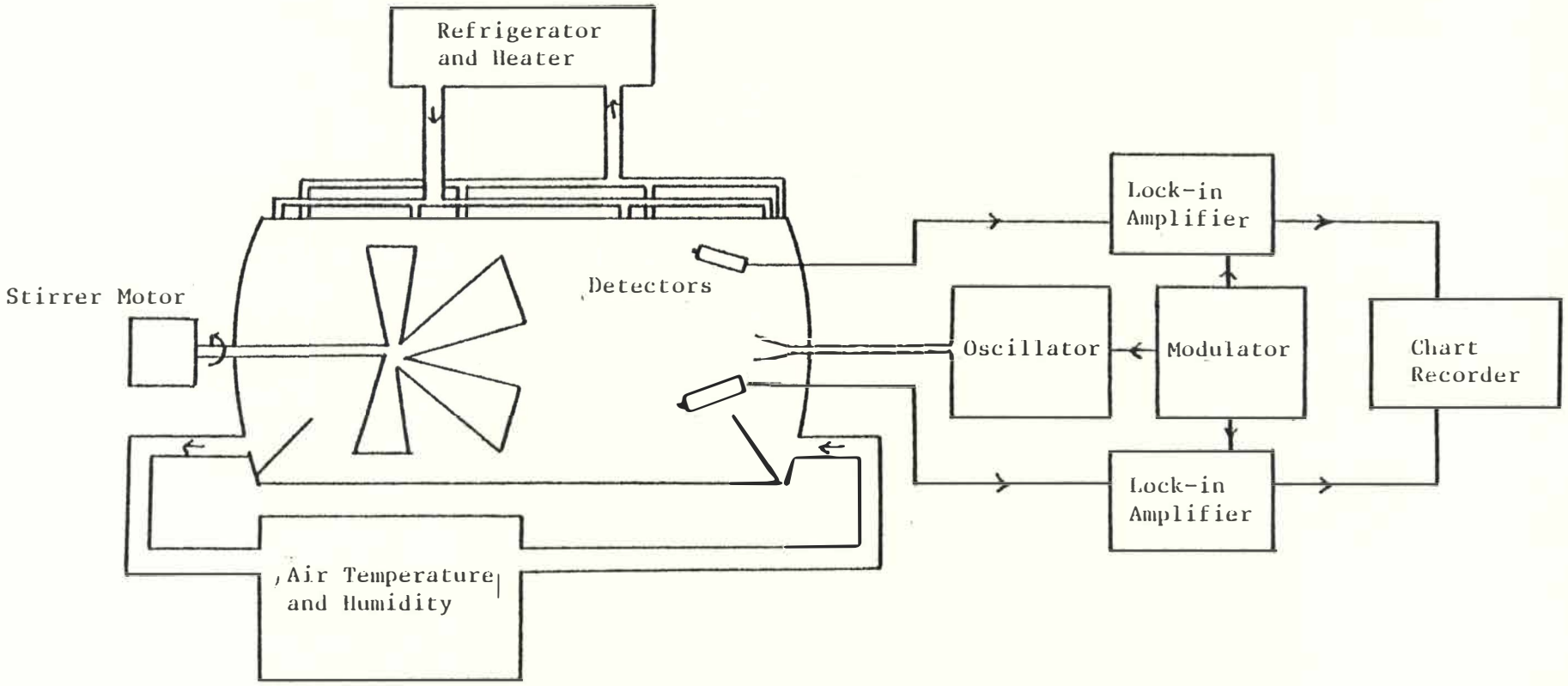

Fig. 3 Layout of Operating System

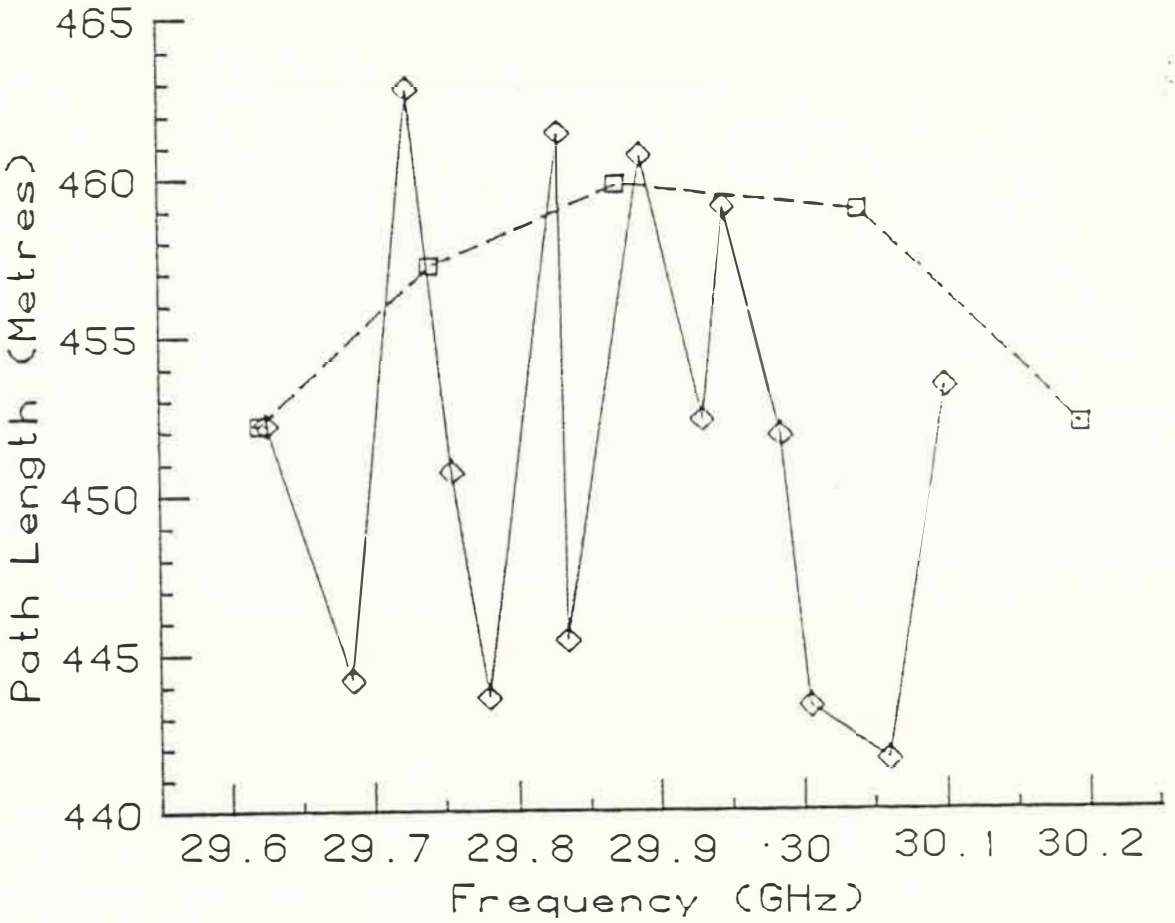

◇ Narrow Bandwidth Source [30 MHz]

□ Wide Bandwidth Source [120 MHz]

Fig. 4 Cavity Pathlength as a Function of Frequency

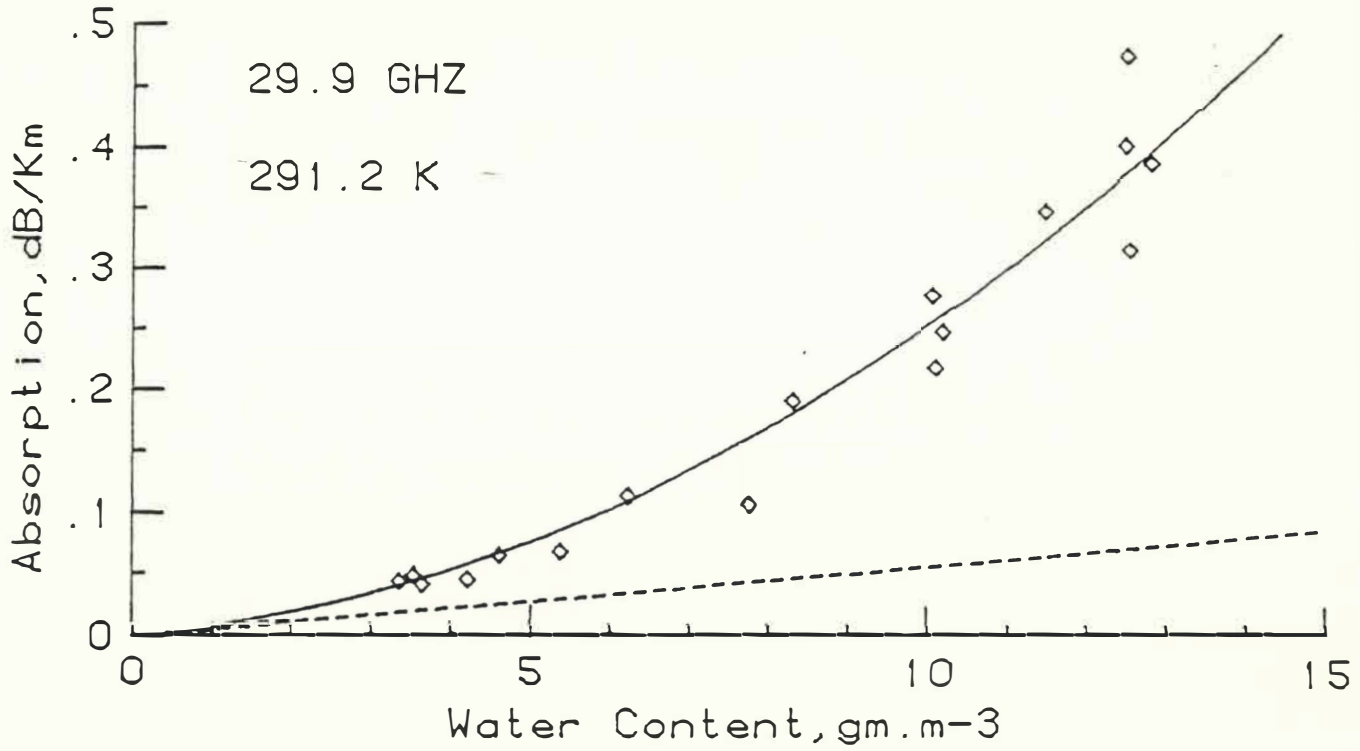

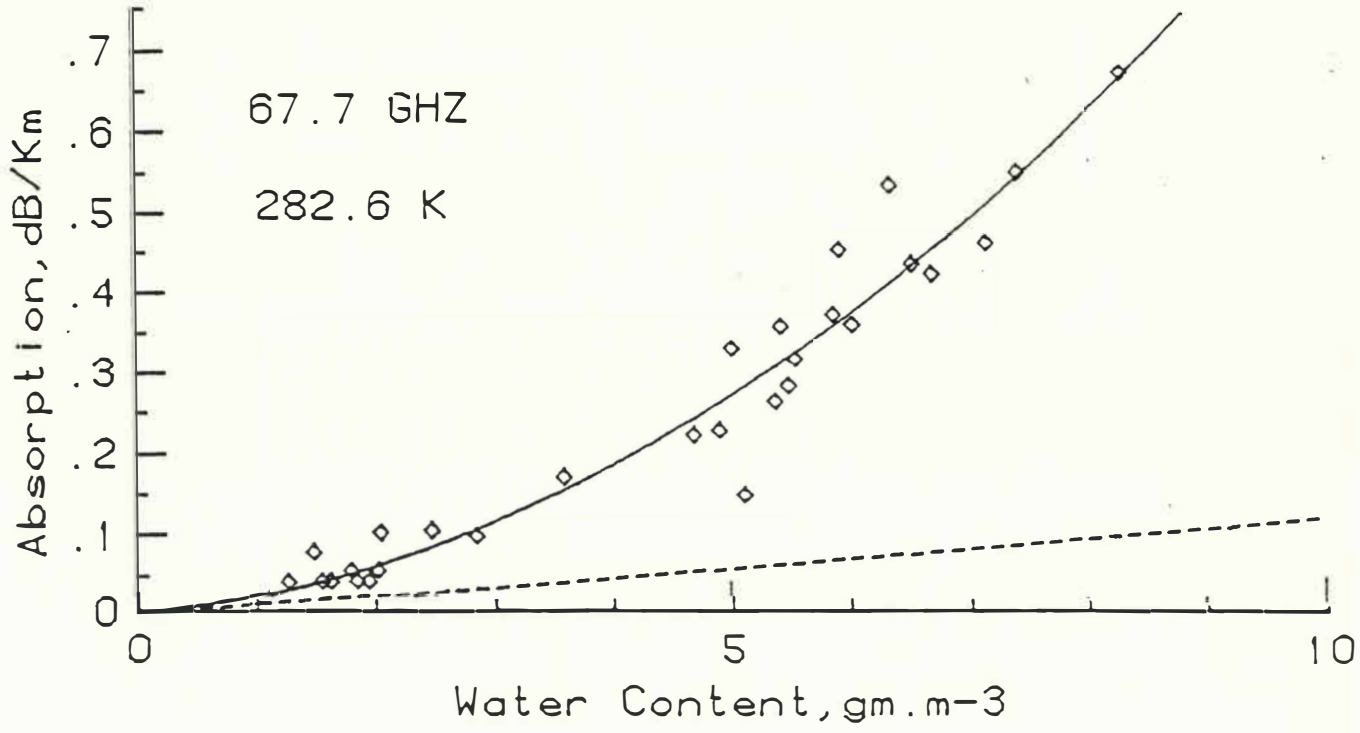

Fig. 5 Pressure Dependence of Excess Absorption

The dotted line is the AFGL prediction

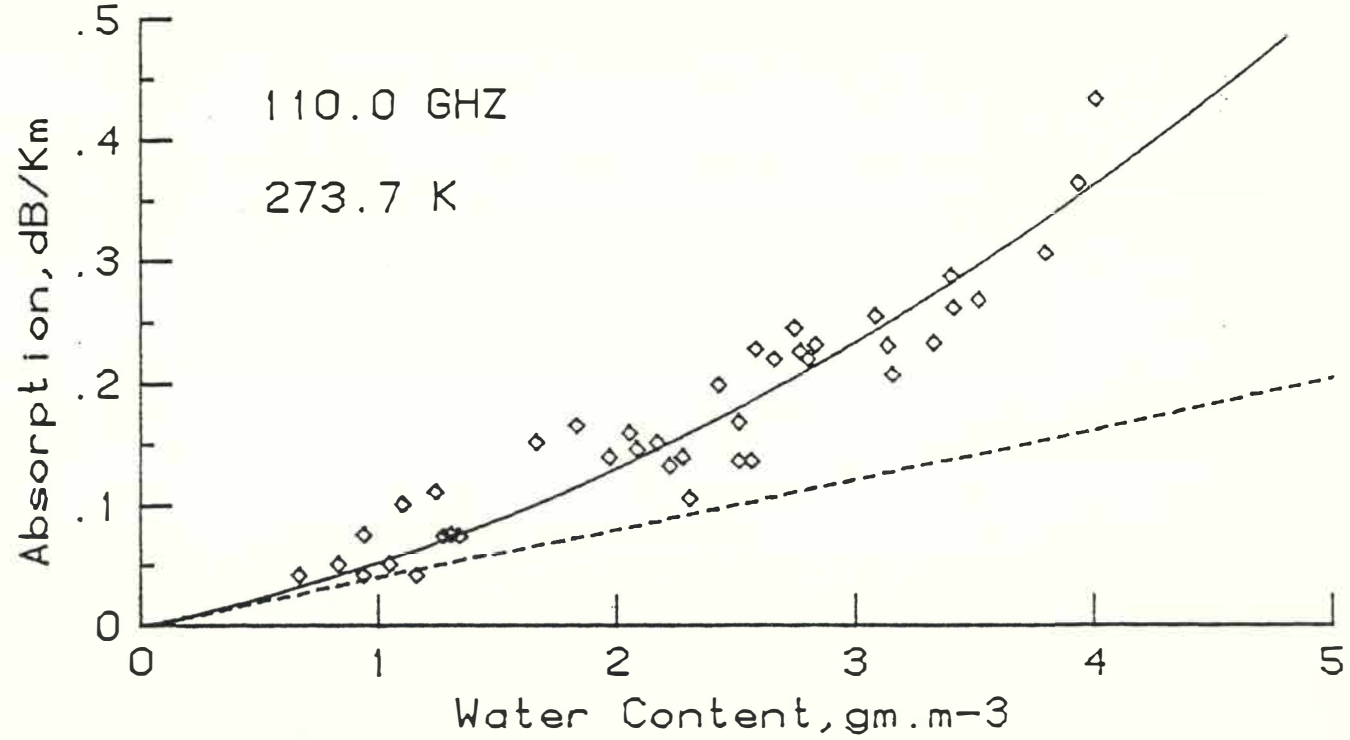

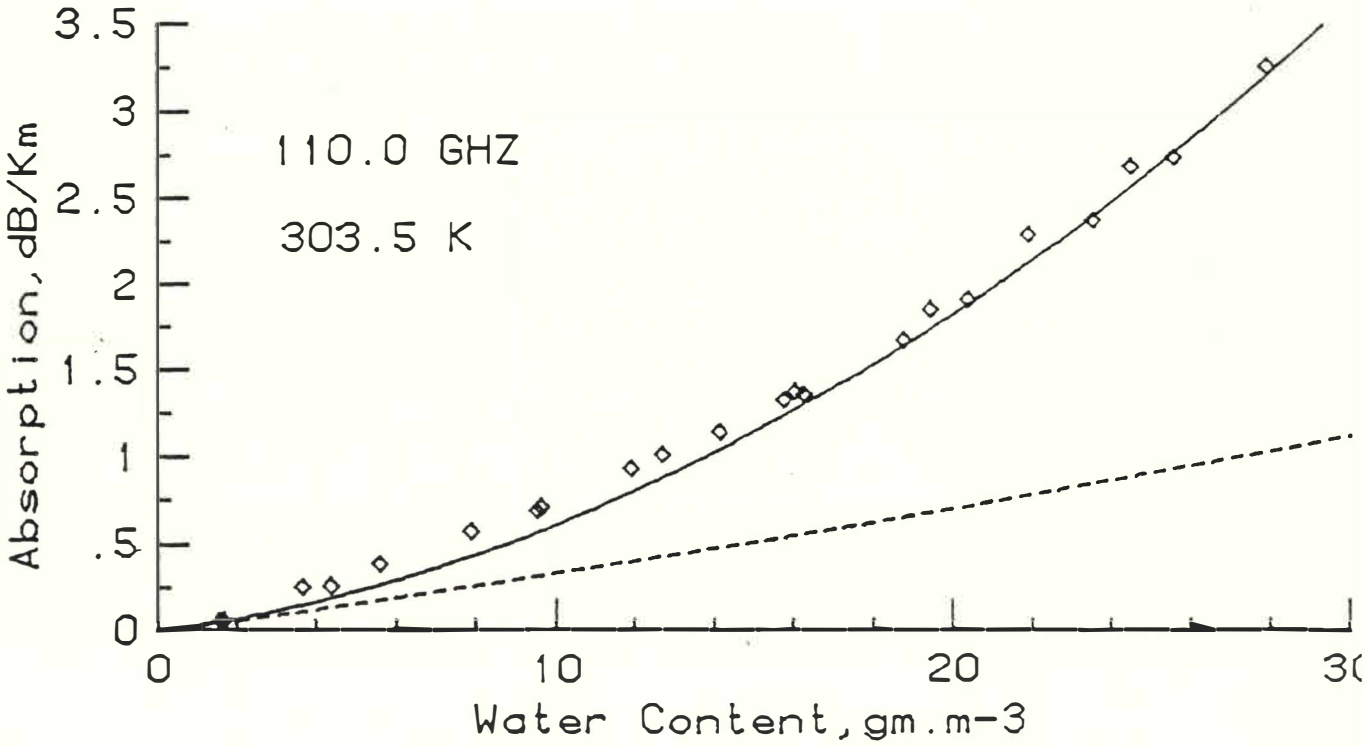

Fig. 6 Pressure Dependence of Excess Absorption

The dotted line is the AFGL prediction

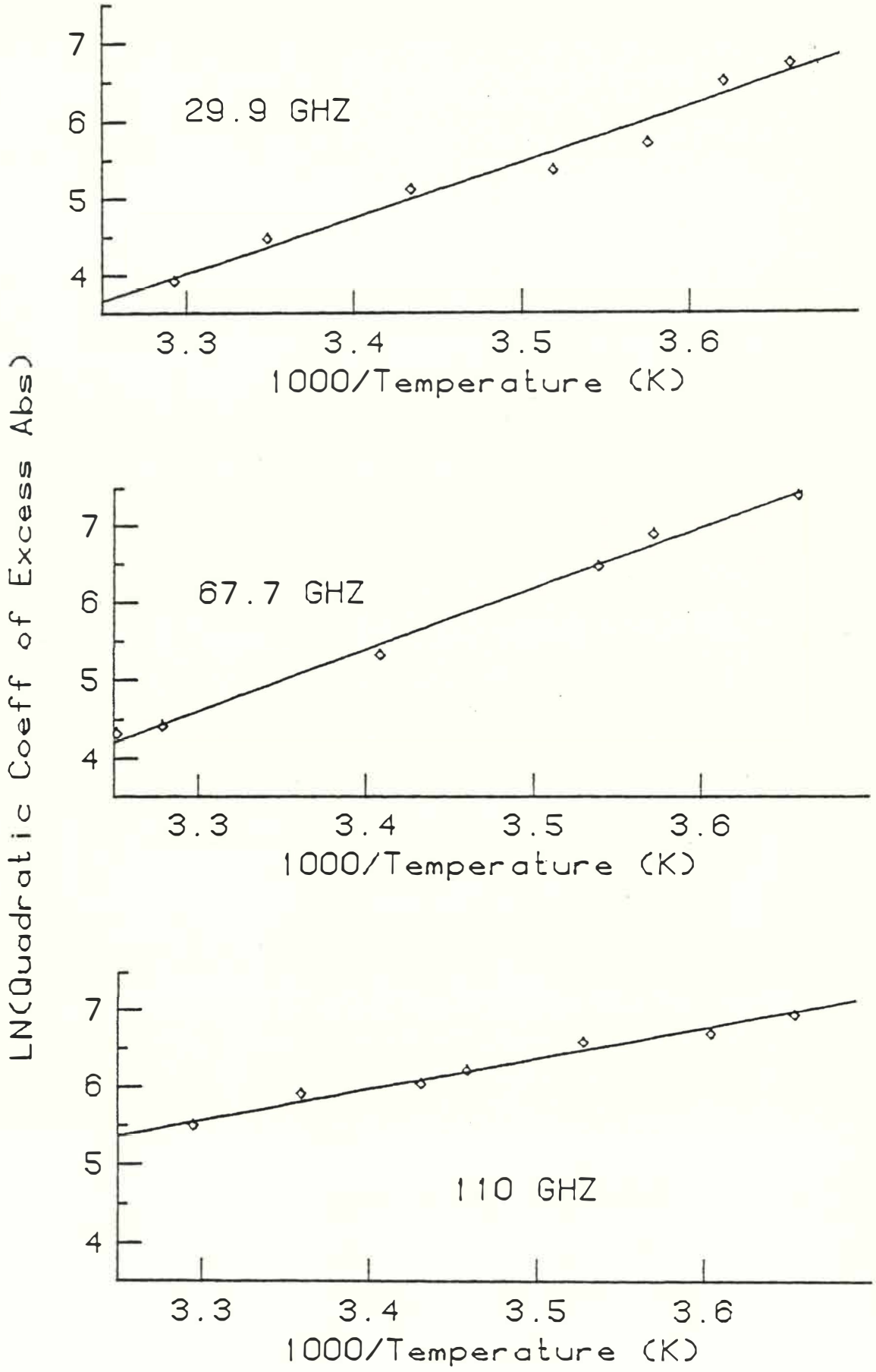

Fig. 7 Temperature Dependence of Excess Absorption

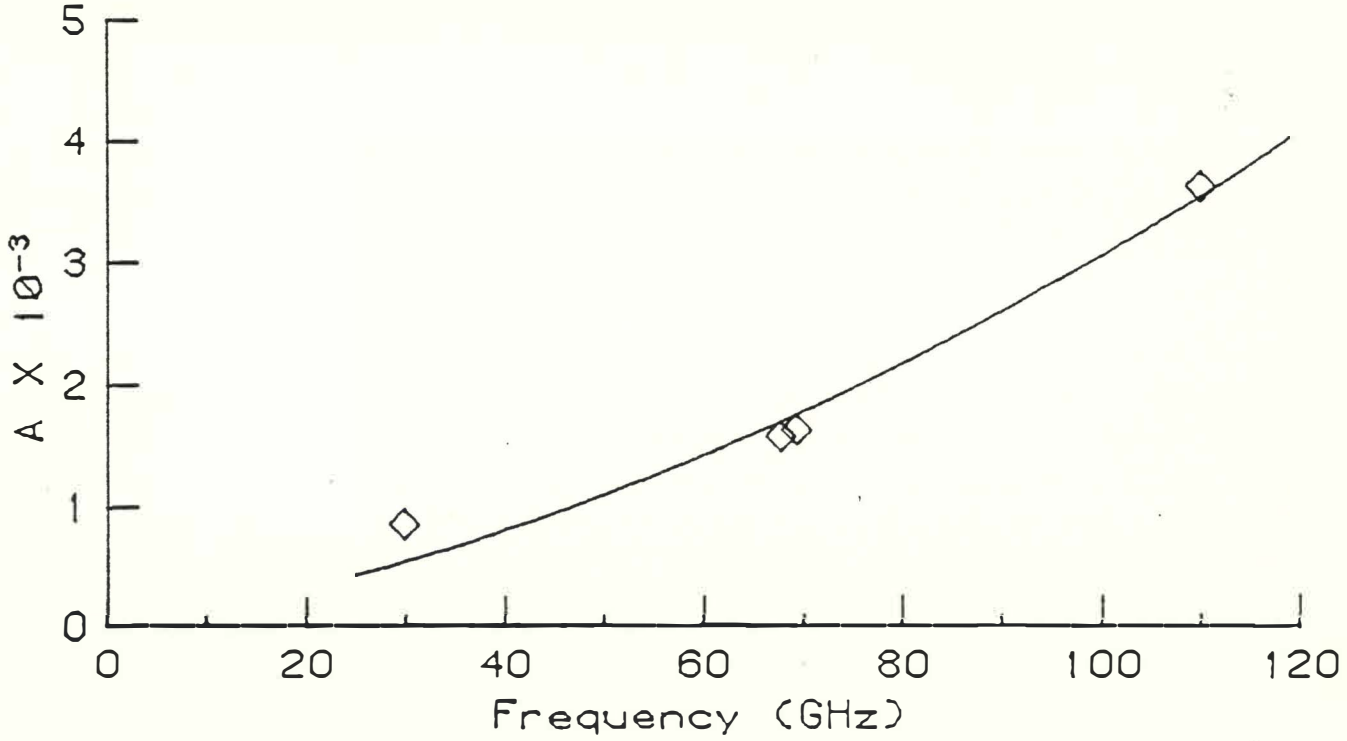

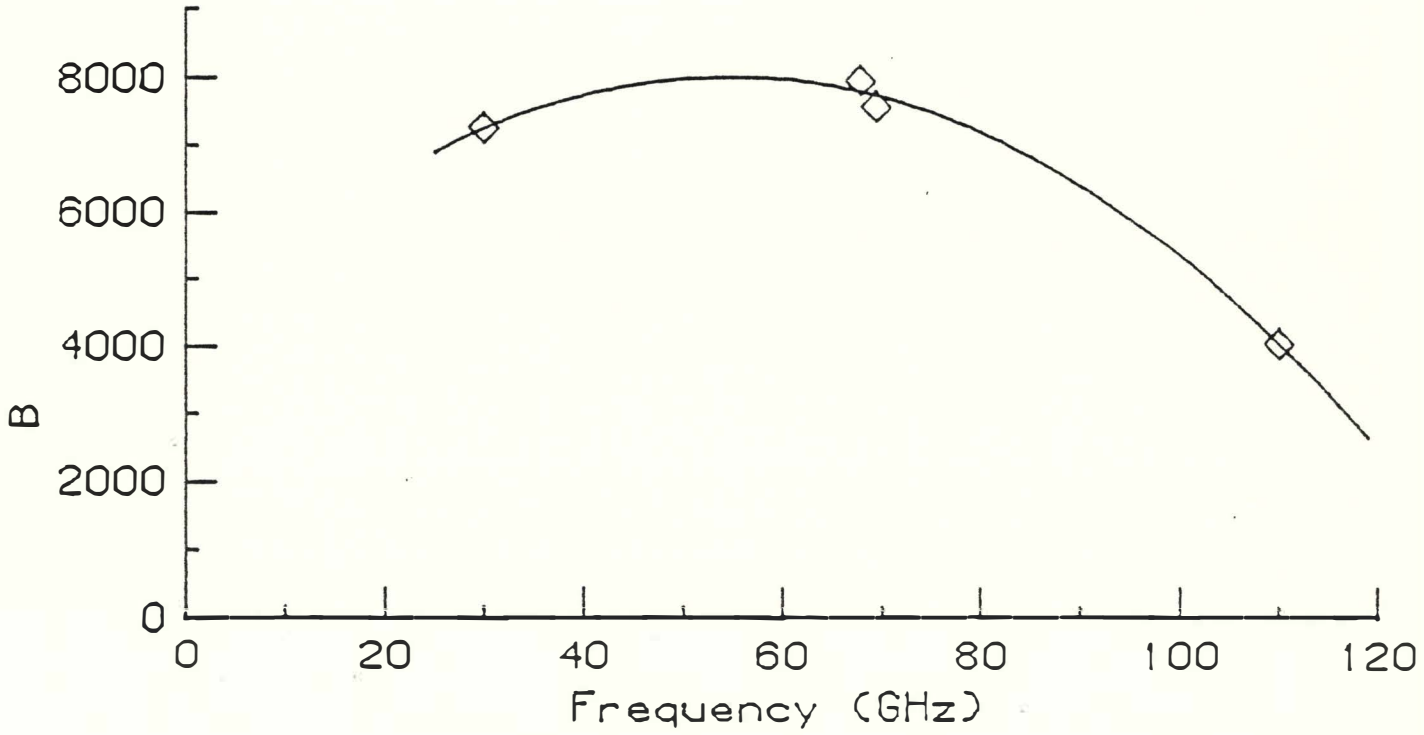

Fig. 8 Fitting of constants in Prediction Equations

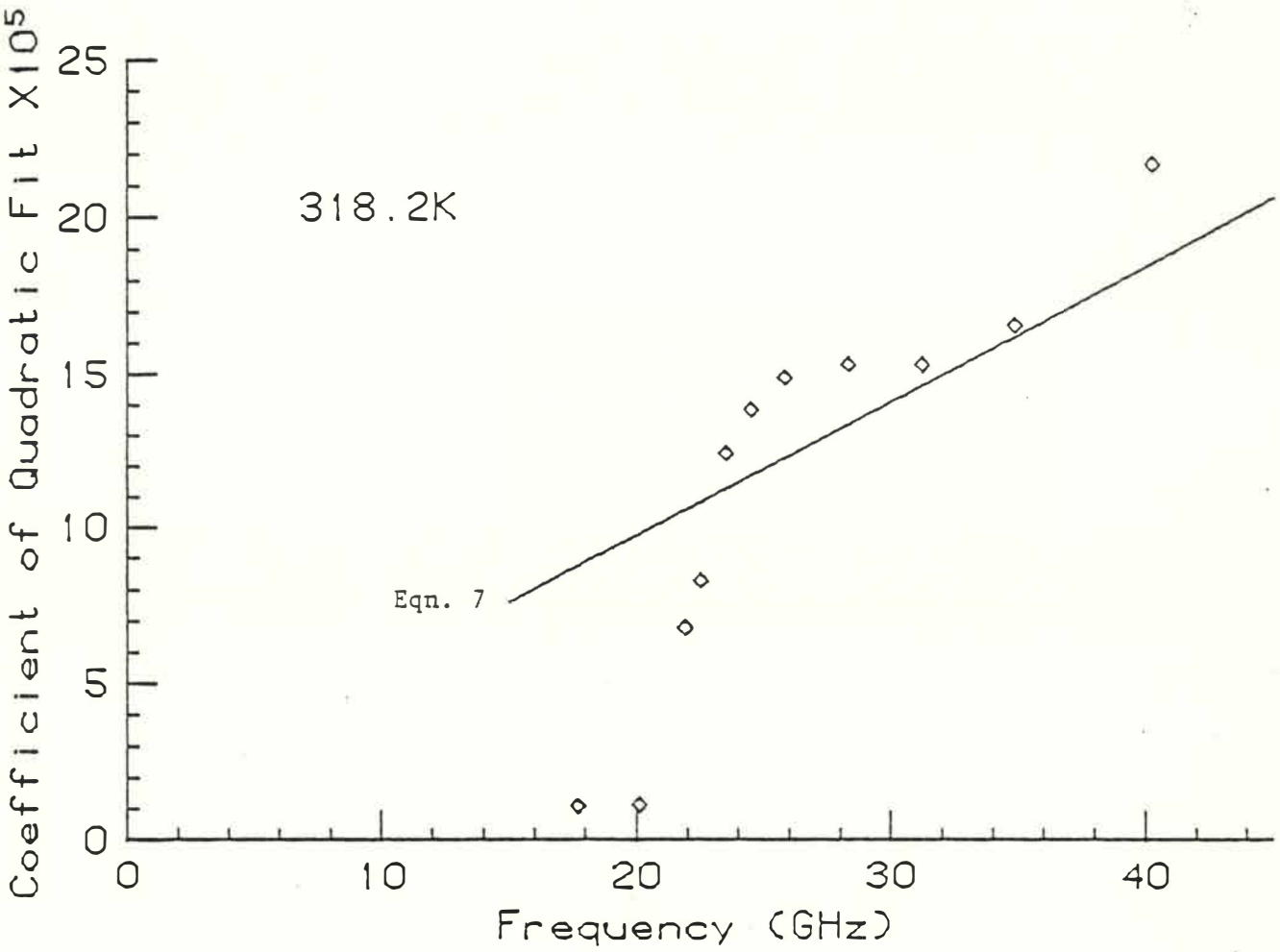

Data points are quadratic fits to
(B & A measured - AFGL prediction)

Fig. 9 Excess Absorption, Becker and Autler (Ref. 11)

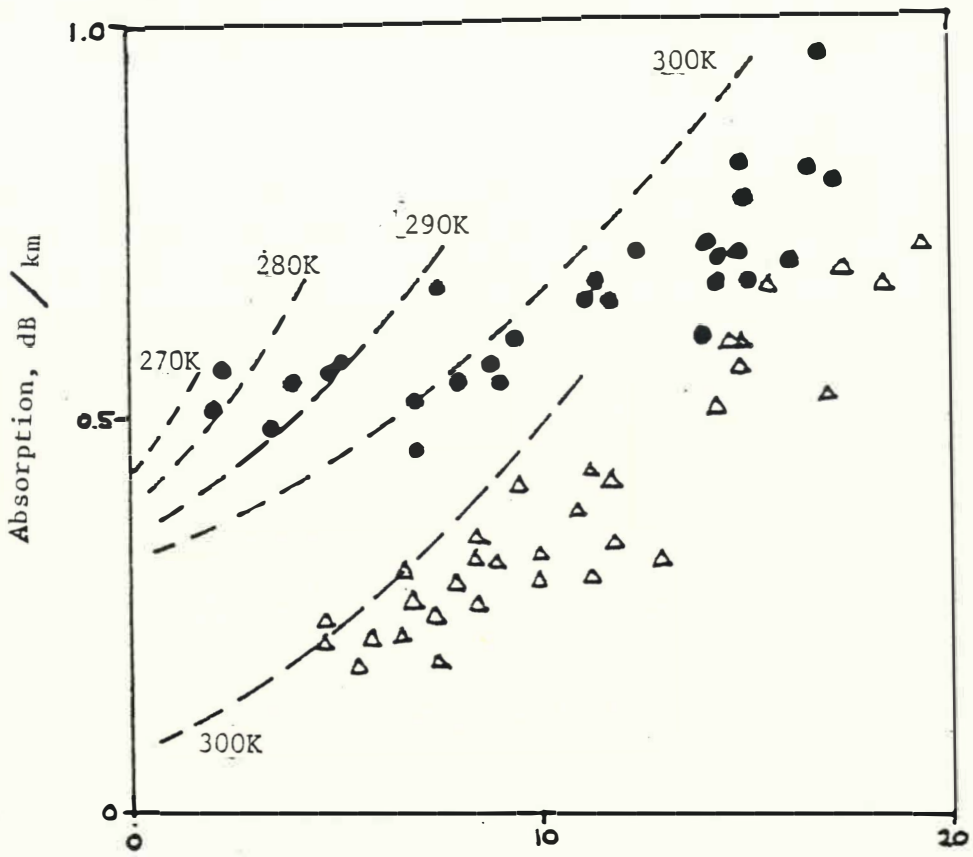

Solid lines are [AFGL prediction + oxygen + Eqn. 7] at the indicated temperature

● 70 GHz

△ 79 GHz

Fig. 10 Horizontal path Absorption, Hogg (Ref. 12)

Fig. 11a Predicted Zenith Attenuation at 110 GHz

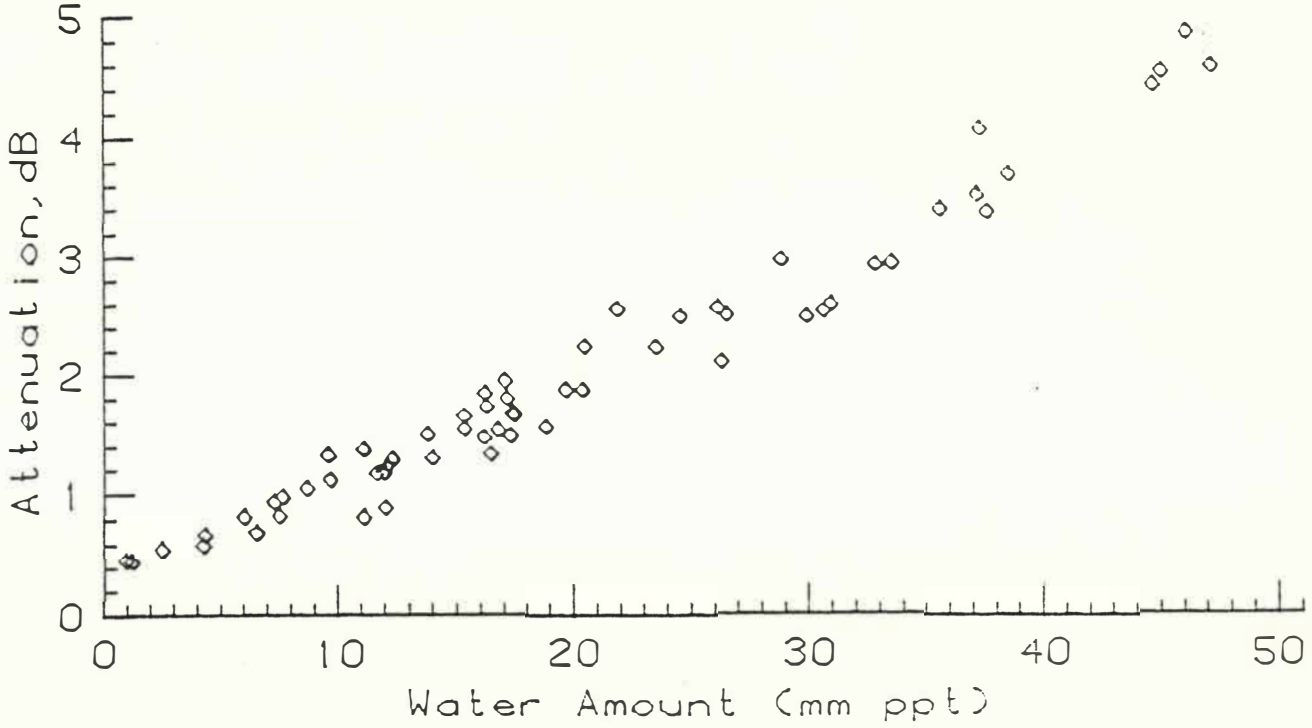

Fig. 11b Measured Zenith Attenuation at 110 GHz

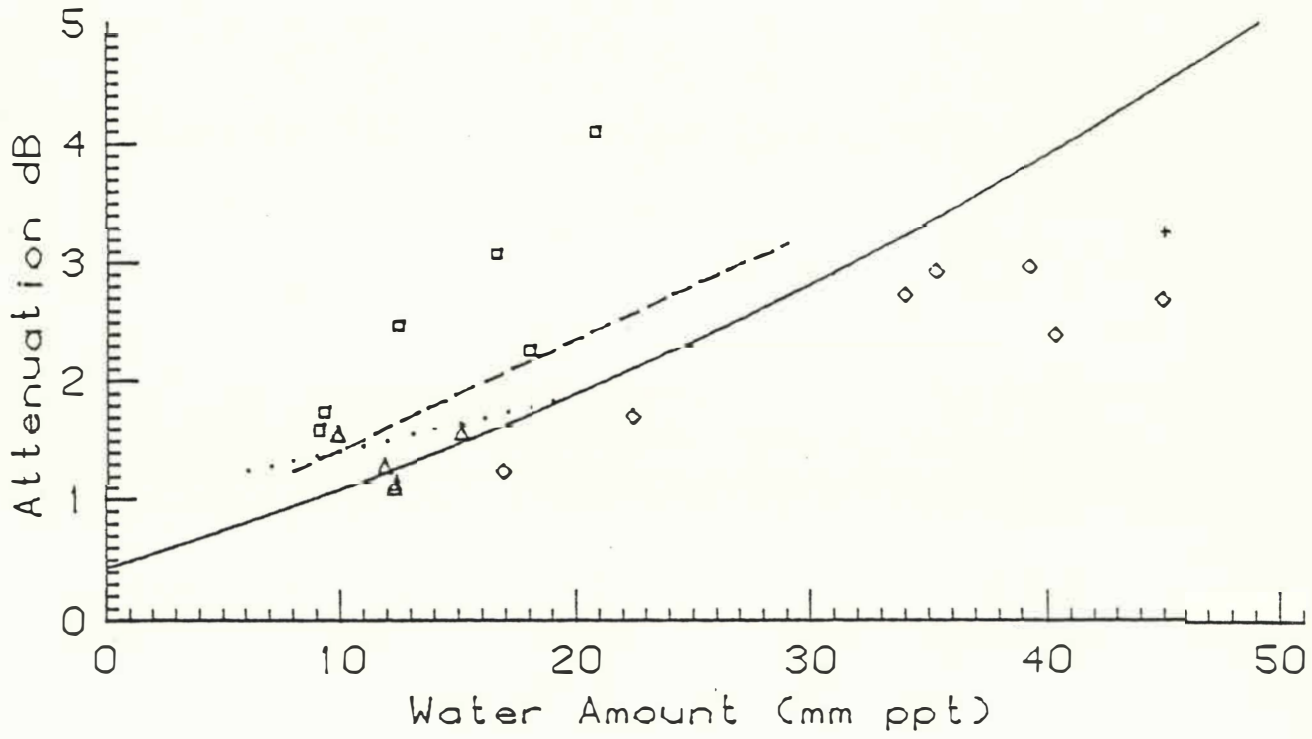

Predicted

Ref. 13

High temp prediction

Ref. 14
[Measured midsummer in Texas]

Ref. 15
[Measured in London]

Ref. 16